Journal of Polymer Research (2022) 29:473
https://doi.org/10.1007/s10965-022-03309-7

ORIGINAL PAPER

Fabrication and characterization as antibacterial effective wound dressing of hollow polylactic acid/polyurethane/silver nanoparticle nanofiber

Sema Samatya Yilmaz[1] · **Ayse Aytac**[1,2]

Received: 15 March 2022 / Accepted: 3 October 2022 / Published online: 20 October 2022

Abstract
In this study, hollow Polylactic Acid/Polyurethane/Silver Nanoparticle (PLA/PU/Ag NP) nanofibers were produced as the antibacterial effective wound dressing against *Escherichia coli*, *Pseudomonas aeruginosa,* and *Staphylococcus aureus*. The produced wound dressings were reported to support the growth of mouse L929 fibroblast cells with cytotoxicity testing. In this way, these antibacterial effective wound dressings, which are predicted to can be used safely in the human body, were produced owning to design that will carry the features of the modern wound dressings. In addition to the development of nanomaterials with high elongation properties by using PLA and PU polymer blends, the fast-drying structures having too high a liquid absorption capacity were obtained owing to the hollow cross-sections of these nanomaterials. As a result of scanning electron microscope analysis (SEM), the surface images of hollow nanofibers were generally smooth, but as the amount of added Ag NP increased, the irregularities, beads, and Ag NP agglomerations along to nanofibers as regional were observed. Moreover, the hollow nanofibers were determined to have quite thin diameters. The surface, chemical, and thermal properties of nanofibers were examined with the Transmission Electron Microscope (TEM), Fourier Transform Infrared Spectroscopy (FTIR), Differential Scanning Calorimetry (DSC), and Thermal Gravimetric Analysis (TGA). Furthermore, it was proved by these analyses that the core of produced nanofibers was successfully removed.

Keywords Antibacterial · Wound dressing · Hollow · PLA/PU blend · Ag NPs · Electrospinning

Introduction

A wound is defined as the temporary or complete loss of the existing physiological properties of the tissues forming skin or mucosa due to the deterioration, or loss of their integrity due to different reasons such as trauma, surgical intervention, or diseases [1]. Cell reproduction is the main element of wound healing [2]. The fibroblast cells come to the wound bed and start collagen synthesis for wound healing [3]. The main point in the modern understanding of wound healing and care is the correct evaluation of the wound, determination of its needs, and keeping the wound moist [2, 3]. A uniform wound dressing may not be the best option for the care of wounds. Wounds can be acute, chronic, exuding, dry or infected, or they can have several features together [4]. For example, if the wound is heavily exuding, it is helpful to use a dressing that can absorb drainage. If the wound is dry, it is more meaningful to choose a product that will keep the environment moist [5]. Composite dressings [6] which are obtained by using both synthetic and natural polymers together are among the modern wound dressings prepared in the presence of active ingredients.

Biocompatibility is an important feature sought in wound dressings [7]. In addition to biocompatibility, biodegradability is also among the desired properties in wound dressings. However, while the polymer degrades, it should not lose its biocompatibility, should not form toxic products, and should have mechanical properties that will provide a suitable environment for the new tissue formed [8].

Among renewable materials, Poly(lactic acid) (PLA) is used often in tissue engineering due to its environmentally friendly features like biodegradability, biocompatibility, and

✉ Ayse Aytac
aaytac@kocaeli.edu.tr; aaytac@gmail.com

[1] Polymer Science and Technology Department, Kocaeli University, Kocaeli, Turkey

[2] Engineering Faculty, Chemical Engineering Department, Kocaeli University, 41380 Izmit/Kocaeli, Turkey

renewability [9]. However, the low toughness of PLA has limited its application areas. Today, polyester/polyether polyol-based thermoplastic polyurethanes with high elasticity features that are compatible with the chemical structure of PLA according to data in the literature are opted to improve the mechanical behaviours of PLA [10–12]. Polyurethane (PU) has excellent mechanical (toughness and strength) features abrasion and chemical resistance to rubber and plastic [13]. Moreover, PU which is known as blood and tissue-compatible polymers is preferred in the medical field [14, 15]. PU which ensures compatibility and comfort owing to its self-healing property has perfect barrier features and oxygen permeability. The good moisture transport properties of PU supply the transport of wound fluid from the contaminated area [16–18]. Nanofiber structures produced from PU [19] and PLA [20, 21] are fully suitable for wound dressing and tissue scaffold fabrication in medical applications because they carry wound dressing nanomaterial properties.

The most up-to-date types of polymeric wound dressings are the nanofiber polymeric structures obtained by the electrospinning method. Compared to conventional membranes, the small pore diameters and very high porosity of nanofiber polymeric materials give the material a breathable structure that prevents the passage of bacteria and substances that can cause infection [22–24]. The cross-section of nanofibers fabricated by traditional electrospinning is generally circular. But today there is a coaxial electrospinning method that may produce hollow cross-section micro/nanofibers as a single material. Hollow nanofibers display superior features compared to solid nanofibers owing to their geometric features [25].

Modern wound dressings, which gain by using additives like silver, zinc, medicine, natural active substances, functionality also by combining the properties, and advantages of synthetic and natural polymers, are promising in terms of treatment. Silver (Ag) since the 1800s, with its antiseptic, anti-inflammatory, and antifungal properties, is used as a broad-spectrum antimicrobial agent in the treatment of burns, wounds, and numerous bacterial infections [26]. Ag does not accumulate in the body. Absorbed Ag is excreted from the body in 2–4 days with 90–99% of the stool and urine. Compared with other silver forms, silver nanoparticles (Ag NPs) showed more effective antimicrobial activity against microorganisms owing to their high surface area. Ag NPs primarily attacks the respiratory chain and prevent cell division, and finally, cell death occurs [27].

In our previous studies, nanofibers were produced from PU/PLA blends and compatibilized PU/PLA blends, and then characterization analyses of the prepared nanomaterials were performed [28, 29].

Our previous study [28] contributed to the literature by producing PLA/PU nanofibers by electrospinning method and examining their properties. PLA polymer, which is biodegradable and biocompatible, but due to its brittleness that limits its use alone, when used together with PU, flexible and durable wound dressing materials were obtained, providing high patient comfort. In other words, while its partial compatibility with blood and non-biodegradable feature limits the use of synthetic PU polymer in the health sector alone, when used with natural PLA polymer, biocompatible and biodegradable nanomaterials with superior mechanical and physical properties were produced.

Besides all this, while the highly hydrophobic character of PLA and PU nanofibers [28] creates a field of use for dry wounds, limited its use for exudative wounds. In order to eliminate the limitation of this contribution to the literature, hollow PLA/PU nanofibers were produced. Due to the idea of modern wound dressing, the appropriate wound dressing design by choosing according to the wound type has been provided in this study.

These hollow PLA/PU/Ag NPs electrospun mats have all the features expected from a modern wound dressing, thanks to the continuity of its ability to absorb excess exudate and dry quickly by providing high absorbency. In addition, while hollow nanofibers prepared with different polymers appeal to different purposes in the literature, the most important difference between our study from other studies is that hollow nanofibers were produced by choosing the wound type and their use as a wound dressing was designed. Hollow PLA/PU/Ag NPs nanofibers were produced in order to provide high absorbency in exuding wounds, hence keeping the wound environment moist and showing rapid healing and antibacterial effect. Thus, the use of hollow PLA/PU nanofibers only on dry wounds has disappeared. Therewithal, it was indicated the antibacterial effect of electrospun wound dressings with hollow PLA/PU/Ag NP will support rapid healing of the wound by destroying the bacteria formed in the wound environment after surgical procedures, injuries, and burn treatments. In this study, it was emphasized that rapid wound healing will be achieved with increased biocompatibility in the presence of Ag NP. Thus, It was enhanced wound dressings that have high flexibility that does not limit the patient's mobility, and mechanical strength enough to protect the wound from external factors.

This paper has been an important study in terms of guiding those hydrophobic nanofibers used for dry wounds or other suitable wounds that can also be used as wound dressings for exuding wounds by making those nanofibers hollow.

To the best of the authors' knowledge, there are no previous studies in the literature, except for our own studies, on the production of hollow and non-hollow PLA/PU/Ag NPs blended electrospun nanofibers. Therefore, the studies associated with hollow, Ag NPs, and different using areas were summarized.

Lee et al. [30] produced porous polymeric hollow nanofibers using coaxial electrospinning. They found

that fiber diameter and wall thickness of hollow fibers were highly affected by solvents and polymer concentrations. The study of Zhang et al. produced single and double hollow cross-section PAN micro/nanofiber with vertical electrospinning. The effect of production parameters on morphology was investigated. Polyvinylpyrrolidone (PVP) was used as an internal solution, and it was removed from the fiber structure [31]. Li and Xia fabricated fibers with shell and core from organic/inorganic polymer or ceramic composites by flowing two immiscible polymer solutions through two capillary needle tips. They removed the core and fabricated hollow nanofibers with only the shell [32]. Khil et al. evaluated the performance of nanofiber surfaces obtained from the electrospinning of PU as a wound dressing. These dressings demonstrated controlled water loss, excellent oxygen permeability, and enhanced fluid drainage ability owing to the porous structure of nanofibers, large surface area, and specific properties of PU [33]. Hajikhani et al. used the PLA/Poly (ethylene oxide) (PEO)/ Cefazolin blend as the core and the PVP/collagen as a shell. It has developed a biodegradable and biocompatible nanomaterial with high mechanical strength. The antimicrobial activity of the scaffold was investigated against *escherichia coli (E.coli), staphylococcus aureus (S.aureus),* and *pseudomonas aeruginosa (P.aeruginosa)* by disc diffusion method. The results showed a high effect on the antimicrobial activity of electro gravity mats [34]. Ag NPs that are highly effective against common infection-causing pathogens, including Gram-positive *S. aureus* and Gram-negative *E. coli*, without inducing drug resistance were used in the studies [35, 36]. Several studies were conducted since the first systematic investigation of the antimicrobial effect of silver by Gibbard [37], and a study in patients with burn injuries confirmed the effective wound healing activities of Ag NPs [38]. In the study of Alippilakkottea et al., outstanding antibacterial properties were observed in the examination of PLA/Ag electrospinning mats against *E. coli* and *S. aureus* by agar disc diffusion treatment. In vitro testing has shown that PLA/Ag mats are compatible with fibroblast cells and do not impair cell growth [39]. In the study by Tijing et al., which is not a hollow nanofiber production, the bicomponent nanofibers were obtained by feeding the PEO-$AgNO_3$ mixture from a syringe and pure PU from another syringe. A certain angle (80°) electrospinning system was used and bicomponent nanofibers were collected as a complex with each other on the plate. The aim of their study was to reduce the $AgNO_3$ in the PEO matrix without a chemical reaction, transform into Ag NPs, and provides a homogeneous distribution of Ag NPs in the PEO matrix. It has been reported that the smaller Ag NPs obtained after the reduction of $AgNO_3$ provide an advantage for antibacterial properties. It was concluded that Ag NP agglomerations or large particles affected negatively antibacterial properties, while homogeneous distributions of small size Ag NPs provide more effective antibacterial properties. Also, the thicker PU nanofibers gave structural stability and prolonged use of the hybrid materials, while the presence of thinner PEO nanofibers provided more reactive surface area. The combination of PU and Ag/PEO bicomponent nanofibers was obtained for antibacterial scaffolds or wound healing applications [40].

This study, it was aimed to fabricate hollow PLA/PU/Ag NPs nanofibers as an antibacterial effective wound dressing. The PLA/PU/Ag NPs nanomaterials were designed especially for exuding wounds according to modern wound dressing properties. Characterization studies of hollow PLA/PU/Ag NPs nanofibers were performed with Scanning Electron Microscope (SEM), Dispersive X-Ray Analysis (EDX), Transmission Electron Microscope (TEM), Fourier Transform Infrared Spectroscopy (FTIR), Thermal Gravimetric Analysis (TGA), Differential Scanning Calorimetry (DSC), Liquid Absorption Capacity (LAC), drying time test and mechanical analysis. As well as the characterization tests, their antibacterial activities were investigated against *E.coli* and *P. aeruginosa* from gram-negative bacteria and *S.aureus* from gram-positive bacteria. In addition, cytotoxicity testing was performed on the mouse fibroblast cell line (L929).

Experimental section

Materials

PLA, trade name 4043D, was purchased from Nature Works. Aromatic polyether-based thermoplastic PU with the trade name Estane®GP52DTNAT055 was obtained from Lubrizol (Velox). PVP polymer was also ensured by Alfa Aesar. Ag NPs purchased from Nanografi were 99.99% pure and 35 nm in size. Chloroform (CF) and dimethylformamide (DMF) solvents were supplied from Merck Company.

Method

Preparation of solutions

Firstly, PLA and PU polymer granules were dried at 80 °C for 12 h in a vacuum oven. Then, 10% concentration of pure PLA and pure PU solutions were prepared in CF/DMF (8/2, v/v) mixture solvent. Pure PLA was completely dissolved in a solvent by mixing for 3 h at room temperature. The mouth of the beaker tightly was closed. The same process was applied to pure PU solution. At the end of 3 h, it was completely dissolved by stirring for another 30 min at 120 °C. The PLA/PU (50/50, w/w) blend solution with 10% concentration was prepared as pure PU solution. According to the total solid amount in the 10% concentration PLA/PU (50/50, w/w) mixture, solutions with 1, 3, and 5 (wt%) Ag NP were

prepared. The preparation process of these solutions was performed by mixing in CF/DMF (8/2, v/v) mixture solvent at once in the same beaker, first at room temperature for 4 h, and then for another 30 min at 120 °C with a magnetic stirrer. The pure PVP solution with 40% concentration was also prepared to realize hollow section nanofiber production. The PVP polymer was dissolved in 100% DMF solvent by mixing with a magnetic stirrer for 3 h at 60 °C. The codes of the studies are given in Table 1.

Coaxial electrospinning process

The prepared solutions were worked in the electrospinning process without waiting. The coaxial (core–shell) bicomponent electrospinning method was used to produce nanofibers with hollow sections. The electrospinning setup used for the studies had two feeding pumps working simultaneously, a single aluminium collector plate, and a single high voltage (max 30 kV) DC device. Both this assembly and the device with a single feed pump were purchased from the Inovenso company. The coaxial nozzle with an outer diameter of 1.6 mm (14G) and an inner diameter of 0.64 mm (22G) used in the study was also supplied from Inovenso. Also, the 0.64 mm (22G) needle tip syringe was used in the single-feed electrospinning production assembly. The electrospinning process was carried out in a closed environment at 65% (±5) relative humidity and room temperature (24 °C ± 2).

Pure PLA, pure PU, and PLA/PU/Ag NPs blend solutions were fed into the nanofiber shell, while pure PVP polymer solution was fed into the nanofiber core. Coaxial electrospinning process parameters were determined as 23 kV voltage, 15 cm distance, and 1.00 mL/h feed rate. This process was continued for 2 h. At the end of this production, bicomponent nanofibers were produced to obtain hollow nanofibers.

In addition, pure PVP nanofiber was obtained from pure PVP solution under the same production conditions by incorporating the device with a single-feed pump into the electrospinning assembly. This fiber was produced to evaluate the analysis results of hollow pure PLA, pure PU, and PLA/PU/Ag NPs nanofibers together with the characteristic properties of pure PVP nanofiber.

The emptying of the inner of pure PLA, pure PU, and PLA/PU/Ag NPs blend nanofibers was achieved by removing the core from the fiber structure using a solvent in which the core nanofiber was dissolved but the shell of the nanofiber was insoluble.

Distilled water was used as the solvent to remove pure PVP fiber from the core of bicomponent nanofibers. Because pure water is not a solvent for PLA and PU polymeric nanofibers. PLA and PU nanofibers are highly hydrophobic [28]. All produced (shell pure PLA, pure PU, PLA/PU/Ag NPs, and core pure PVP) bicomponent nanofibers have waited in distilled water at room temperature for 30 min. It was noticed that the core PVP nanofiber dissolved very quickly and in a short time. So, the hollow parts were filled with water at the same time. All evacuated nanofibers were left to dry at room temperature for 24 h in a dark, closed, and ventilated environment.

The pure PVP nanofiber in the core of the bicomponent nanofiber has an important polymeric structure for this study. Both DMF and distilled water are known as good solvents for dissolving the PVP polymer. The pure PVP polymer solution was dissolved in the presence of 100% pure DMF to be used in the coaxial electrospinning process. Because the pure PVP solution prepared in this way was compatible with the solvent of pure PLA, pure PU, and PLA/PU/Ag NPs solutions. Otherwise, when solutions with different kinds of solvents (like DMF, CF, and distilled water) meet at the outlet of the coaxial nozzle head during electrospinning, it may cause some problems such as polymer freezing, polymer dripping, clogging of the apparatus during jet formation. Seeing these problems can be avoided with PVP polymer, which was used in this study.

Table 1 The codes and content of the studies

Codes of Studies	Core	Ag NPs (%)	Shell (%)	Concentration (%)
HPU	**40 wt% Pure PVP**	-	PU (100)	10
HPLA		-	PLA (100)	
H5PLA5PU		0	PLA/PU (50/50) (w/w)	
H1Ag5PLA5PU		1		
H3Ag5PLA5PU		3		
H5Ag5PLA5PU		5		

Characterization

Three-dimensional images of the obtained hollow nanofiber surface and fiber diameter measurements were performed with a QUANTA 400F Field Emission Scanning Electron Microscope (SEM). Moreover, Energy Dispersive X-Ray Analysis (EDX) has been performed together with SEM analysis. So, the amount of Ag elements in the structure of hollow nanofibers has been determined as the percentage. At the same time, high-resolution surface images were obtained by making the detailed two-dimensional surface examination of hollow nanofibers with FEI 120 kV HCTEM brand Transmission Electron Microscope (TEM). With TEM surface images, it has been proven that the hollow section nanofiber structures are hollow. TEM samples were also meticulously prepared by us. After PVP removal, the hollow nanofibers have been placed on a 3 mm diameter grid (multi-porous copper grid) as a very fine structure.

The conductivity value of all solutions has been measured at 24 °C (± 2) by the Mettler Toledo liquid conductivity meter. Chemical structure analysis of hollow nanofibers was performed with ATR unit spectrometric Perkin Elmer Spectrum 100 Fourier Transform Infrared Spectroscopy (FTIR) device in the range of 650–4000 cm^{-1}.

Thermal gravimetric analysis (TGA) was performed with the Mettler Toledo TGA 1 device at a heating rate of 10 °C/min and a temperature range of 25 °C to 600 °C. Differential scanning calorimetry (DSC) analysis was performed in a single step with the Mettler Toledo DSC 1 device at a heating rate of 10 °C/min and a temperature range of (-50 °C)—300 °C. During the thermal analyses (both TGA and DSC), high-purity nitrogen gas has been sent to the system at a flow rate of 30 ml/min.

The mechanical properties of hollow nanofibers were investigated with a Lloyd Instruments LRX Plus brand drawing device at 1:10 mm/min drawing speed and 5kN load by ASTM D882 standard. For the tensile test, 5 nanofibers of 50 mm × 15 mm dimensions were tested from each hollow nanofiber and their averages were taken. The error bars given in the analysis results represent the standard deviations.

Liquid absorption capacity and drying time tests

The liquid absorption capacity (%) of hollow nanofibers was realized by the EDANA 10.3.99 standard in environmental conditions. Firstly, hollow mats were cut with dimensions of 1 cm × 1 cm. Then, their dry weights were weighed on a precision balance and noted. Samples were settled into the beaker containing 50 mL of distilled water, suspended at the midpoint of the beaker, and waited for 1 min. Then, the hollow nanofibers were removed from the beaker with the help of tweezers. Both surfaces of nanofibers were kept on filter paper for 5 s and the first liquid on the mats was taken. Later, the wet nanofibers were then weighed. The liquid absorption capacity (LAC) of nanofibers according to the initial dry weight and subsequent wet weight ratios (%) were calculated according to the following "Equality (1)":

$$LAC(\%) = \frac{N_s - N_k}{N_k} x100 \quad (1)$$

where N_s refers to the weight of wet nanofibers; N_k is the initial dry weight of the nanofibers. Tests were repeated 5 times for each sample and the average of the obtained values was evaluated.

For the drying time (minute, min.) test, hollow nanofibers were prepared as 1 cm × 1 cm and 0.1 mL of distilled water was dropped on the hollow nanofibers from 1 cm above, and drying times were observed. Since nanofiber samples are quite light, intermediate weights are not included in the calculation. The weights of wet nanofibers were measured on a precision balance every 1 min (60 s). For the time when the nanofibers fully return to their original weight test is terminated. Tests were repeated 3 times for each mat and the average of the times was appreciated.

In-vitro antibacterial test

Agar plate colony counting which is a quantitative method [41–43], was used to examine the antibacterial activity of the PLA/PU/Ag NPs nanofibers. This test was performed appropriately to the AATCC-100 standard [44, 45].

The in vitro antibacterial activity test was fulfilled against *S. aureus* (ATCC 29,213) which is a Gram-positive bacterium and *P. aeruginosa* (ATCC 27,853) and *E. coli* (ATCC 25,922) which are Gram-negative bacteria with agar plate colony counting method.

Mueller Hinton Agar (MHA) and Mueller Hinton Broth (MHB) (Merck, Germany) prepared accordingly the fabricator's explanations and were sterilized in an autoclave for 15 min at 121 °C. Bacteria were cultivated overnight on MHA at 37 °C. Colonies of bacteria grown on MHA were suspended in 3 ml MHB and turbidity was adjusted to 0.5 McFarland ($1{,}5 \times 10^8$ CFU ml^{-1}) in MHB.

The bacterial suspension was afterward diluted tenfold with saline (0.9% NaCl) to a concentration of 10^4 CFU ml^{-1}. Antibacterial test nanofibers were prepared from 3 different regions of each nanofiber. To study the antibacterial activity of samples, all hollow nanofibers were cut as sized 1 cm × 1 cm, and afterward, both surfaces of the nanofibers were sterilized under UV light for 30 min each. Then, each sterile sample was placed in a 24-well plate and 600 µl of prepared bacterial suspension (10^4 CFU mL^{-1}) was inoculated into each well. After, it was inoculated in 20 µL MHA from each well at 0 h, 6 h, 12 h, and, 24 h and incubated overnight at 37 °C. End of this time, agar plates were counted. So, each cultivation, fulfilled at the times specified for each different bacterium type, was repeated three times for each nanofiber. The antibacterial activity (%) of hollow nanofibers [41–43] was calculated according to the following "Equality (2)":

$$Antibacterial\ Activity\ (\%) = (A - B)/A \times 100 \quad (2)$$

where A is the average colony number of the untreated hollow nanofiber control sample; B is the average number of colonies per hour with the least number of colonies except the 0 h. At the same time, the standard deviations (std. dev.) were calculated.

Cytotoxicity test

By the direct contact test, the cytotoxicity of the hollow nanofibers was performed with the WST-1 test for the mouse fibroblast cell line (L929) [39, 46, 47].

In-house apparatuses (diameter: 9 mm, inner open surface area: 0.63 cm^2) were styled to fasten up the hollow nanofibers in the well of a 24-well plate. These apparatuses were sterilized in an autoclave for 15 min at 121 °C. Each side of the hollow nanofibers was sterilized for 30 min each, under UV light. L929 cells were cultured in high glucose DMEM supplemented with 10% fetal bovine serum, 1.4% L-glutamine, 100 U/mL penicillin, and 100 ug/mL streptomycin. Also, L929 cells were first seeded in apparatuses (7×10^4 cells/splice) implanting hollow nanofibers in a 24-well plate. The seeded well plate was afterward cultured at 37 °C and 5% CO_2. Following 24 h of incubation, 50 µL of WST-1 solution (BioVision Incorporated, USA) was supplemented to each well and the plate was incubated at 37 °C for 2 h and then shaken well for 1 min. Later, the measurement of OD has performed at the wavelength 450 nm with a microplate reader (Multiskan FC, Thermo Scientific). These measurements were repeated 3 times and the average values were reported. The error bars given in the graphic results represent the standard deviations. Cell viability (%) was calculated according to the following "Equality (3)":

$$Cell\ vailabilty\ \% = \frac{A_b\ sample - A_b\ blank}{A_b\ control - A_b\ blank} \times 100 \quad (3)$$

A_b *sample* is the absorbance of the hollow nanofiber, A_b *blank* is the absorbance of the blank, A_b *control* is the absorbance of the negative control.

Cells in the apparatus without including hollow nanofibers were cultured as the negative control. The cells in the insert with 1% (v/v) Triton X-100 (Sigma) and 500 µg/ml Geneticin (Gibco) as a positive control, and an equal volume of culture medium that contained WST-1/ECS solution in an empty well as a blank were prepared.

Result and discussion

SEM and TEM micrographs of hollow PLA/PU/Ag NPs nanofibers

SEM surface images of Ag NP doped hollow PLA/PU nanofibers at 2000 × magnification and 50 µm scale are shown in Fig. 1. It has been observed that the H5PLA5PU nanofiber has a bead-free and smooth fiber structure. As the Ag NP ratio added to the structure increased, the irregularities and bead structure formation in the nanofiber gradually increased. Because the conductivity of the solutions has increased with an increase in the amount of Ag NP added. The conductivity measurements of prepared solutions are given in Table 2. As the conductivity of the solutions increases, surface tensions are expected to decrease. During the electrospinning process, when the applied voltage value is exceeded to overcome the surface tension of the solutions, the polymer jet will extend, and without-beads thinner fibers will be formed. However, if the optimum voltage value applied for thin fiber formation is further increased, beaded structures will begin to be observed due to the high voltage. Production parameters were kept constant in this study. It was concluded that the constant voltage value applied to overcome the decreasing surface tension of the solutions with the addition of Ag NP is high. In this case, while bead structures on nanofibers were observed, it has been determined that the nanofiber diameters were decreased.

The dark images obtained from the SEM analysis are shown in Fig. 2, and the distribution of Ag NPs on the nanofibers has been observed. The Ag NP agglomerations on H5Ag5PLA5PU nanofiber are given in Fig. 2d. The Ag NP agglomerations were seen especially on the beads of nanofibers. However, the distribution was observed generally homogeneous on 1% doped Ag NPs. The reason for the agglomerations was associated with the high density of Ag NPs. Because while the density of silver is 10,49 gr/cm^3, the densities of PLA and PU are approximately 1.25 gr/cm^3. Thus, the distribution of high-density Ag NPs in polymers with low density becomes difficult and occurred local agglomerations.

Average fiber diameter values of hollow PLA/PU/Ag NP nanofibers are given in Fig. 3. The average fiber diameter of the H5PLA5PU nanofiber was measured as 518 nm. In this study, high-density Ag NPs were added to the PLA/PU (50/50, w/w) blend while keeping the concentration of the solution constant. Considering that there is a linear relationship between density and viscosity, it has been interpreted that the solution viscosities increased with adding of Ag NP. In this case, with the addition of Ag NPs to the H5PLA5PU blends, first an increase and then a decrease in nanofiber diameters are observed. The H5Ag5PLA5PU mat was obtained as the thinnest nanofiber with a diameter average value of 484 nm but having beads along the fiber surface. As for as the H3Ag5PLA5PU nanofiber with an average diameter of 638 nm was viewed to have a less bead structure. It has been observed that among the produced Ag NPs doped nanofibers, the fiber with the smoothest and bead-free surface appearance is the H1Ag5PLA5PU nanofiber with a 736 nm value. For this reason, 1% Ag added PLA/PU mixed solution has been considered to have optimum conductivity depending on the constant voltage value in the production. In addition, the viscosity of the H1Ag5PLA5PU blend was

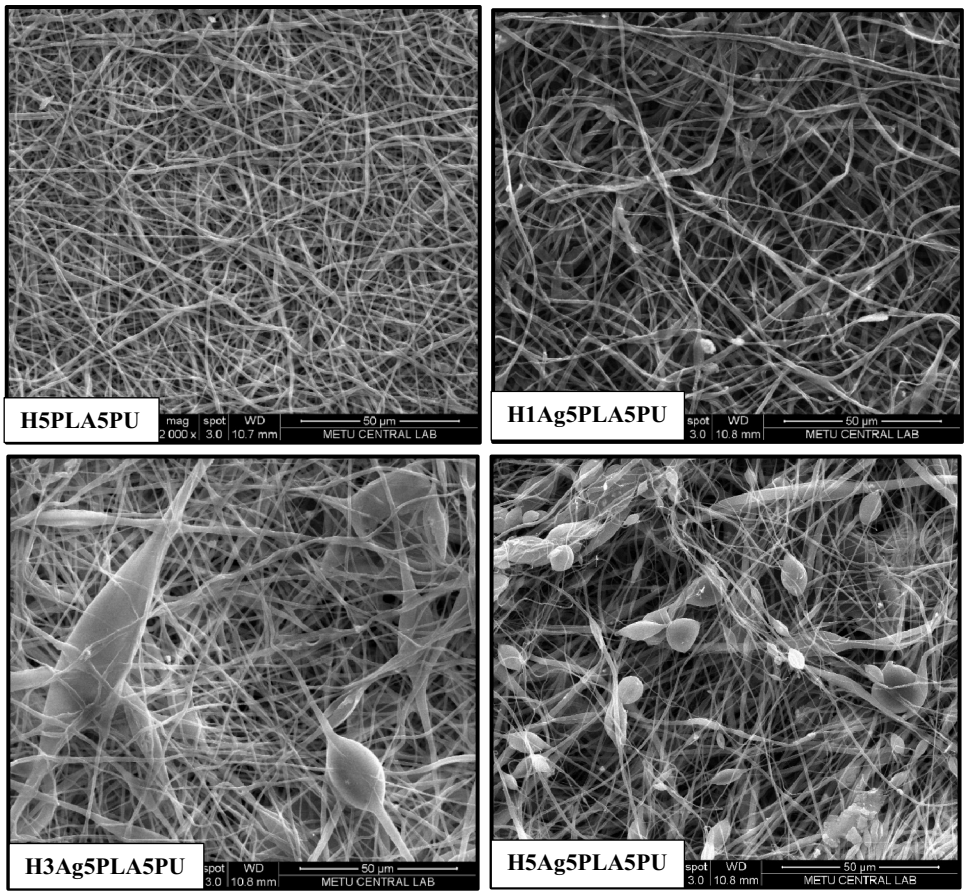

Fig. 1 SEM images of hollow nanofibers (Scale: 50 µm, Mag: 2000x)

determined as the most suitable for the kept constant electrospinning production conditions.

Figure 4 has showed the TEM image expressing the outer diameter measurement and the internal hollow diameter of the thinnest H5Ag5PLA5PU nanofiber. The diameters of the hollows of H5Ag5PLA5PU nanofiber have been measured as 175 (± 2) nm. The transparent inner of the hollow structure compared to the solid structure has been displayed with the contrast difference with TEM analysis. At the same time, it has been proven that the nanofibers are hollow.

EDX analysis results for the Ag element of Ag NP doped hollow PLA/PU nanofibers are given in Table 3. The percentage amount of Ag NP added to the solutions and the percentage amount of Ag NP in the nanofibers were confirmed by EDX results. Ag element content of H1Ag5PLA5PU, H3Ag5PLA5PU, and H5Ag5PLA5PU nanofibers was determined as 1.12, 3.49, and 5.63 (wt%) respectively.

Table 2 The conductivity values of the prepared solutions

Samples	Solution Conductivity (µS/cm) (± 0,1)
Pure CF	0.00
Pure DMF	3.70
8CF/2DMF	0.30
Pure PU	0.30
Pure PLA	0.30
H5PLA5PU	0.30
H1Ag5PLA5PU	0.37
H3Ag5PLA5PU	0.60
H5Ag5PLA5PU	0.78

FTIR analysis of hollow PLA/PU/Ag NPs nanofiber

The graphs of the FTIR analysis of Ag NP doped hollow PLA/PU nanofibers are shown in Fig. 5. The characteristic peak of HPU nanofiber is 1600 cm^{-1} and belongs to aromatic C = O group oscillations. Other peaks of pure PU nanofiber were observed as NH group vibration at 3313 cm^{-1}, as CH2 group at 2858 cm^{-1}, as C = O group vibration at 1704 cm^{-1}, and at 1311 cm^{-1} peak as (NH) + (CN) + (CH) group. The FTIR spectra of HPU showed that the 1263 cm^{-1} peak (C–O–C) belonged to the carbonyl group, the 1084 cm^{-1} peak (C-O–H) vibrations and the 2940 cm^{-1} peak belonged to the CH_2 tensile vibration.

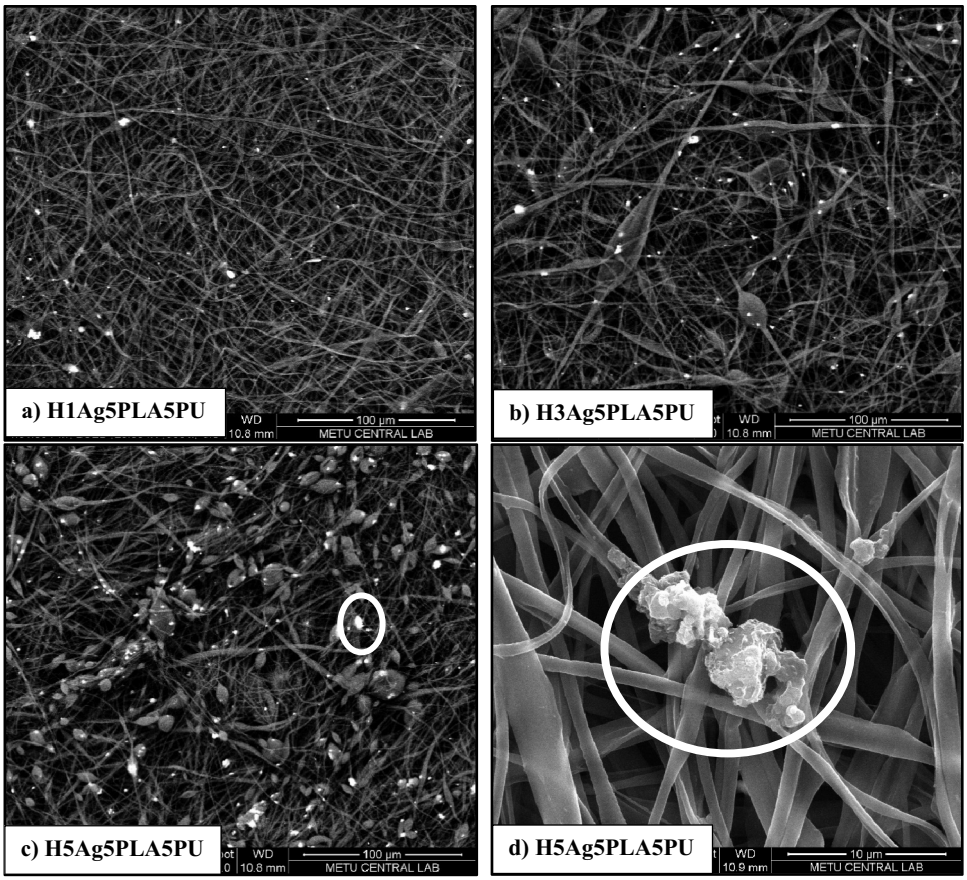

Fig. 2 SEM dark surface images of hollow nanofibers. (Scale: 100 µm, Mag:1000x, for **a**, **b**, **b**. and Scale: 10 µm, Mag:10000x, for **d**.)

The characteristic peak of HPLA is the C = O stress vibration at 1753 cm^{-1}. Other peaks of HPLA fiber were seen at 1449 cm^{-1} for the CH_3 group and at 1367 cm^{-1} for the CH_3 group. The peak of C-N = O group at 1532 cm^{-1} and the peak of C = O–H group seen at 1670 cm^{-1} seen in both pure PLA and pure PU were observed in all PLA/PU nanofibers. All chemical bond peaks of HPU and HPLA nanofibers were also observed in Ag NP-doped hollow nanofibers.

The characteristic peaks of pure PVP nanofiber are the peaks seen at 1650 cm^{-1} (C = O carbonyl group), 1429 cm^{-1} (OH bending), 1373 cm^{-1} (lactone structure) and 1277 cm^{-1} (C = N stretch) [48, 49]. Also, the 3416 cm^{-1} peak denotes

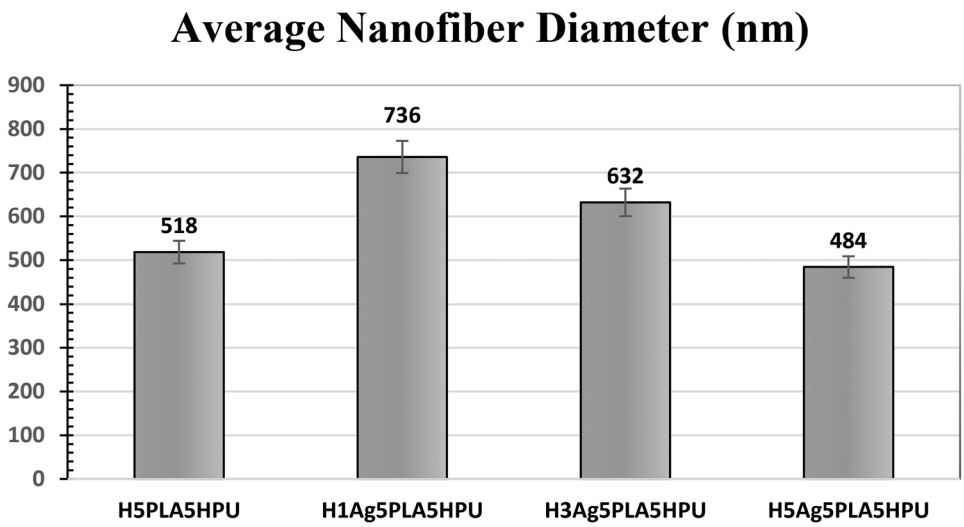

Fig. 3 Average diameter values of hollow nanofibers

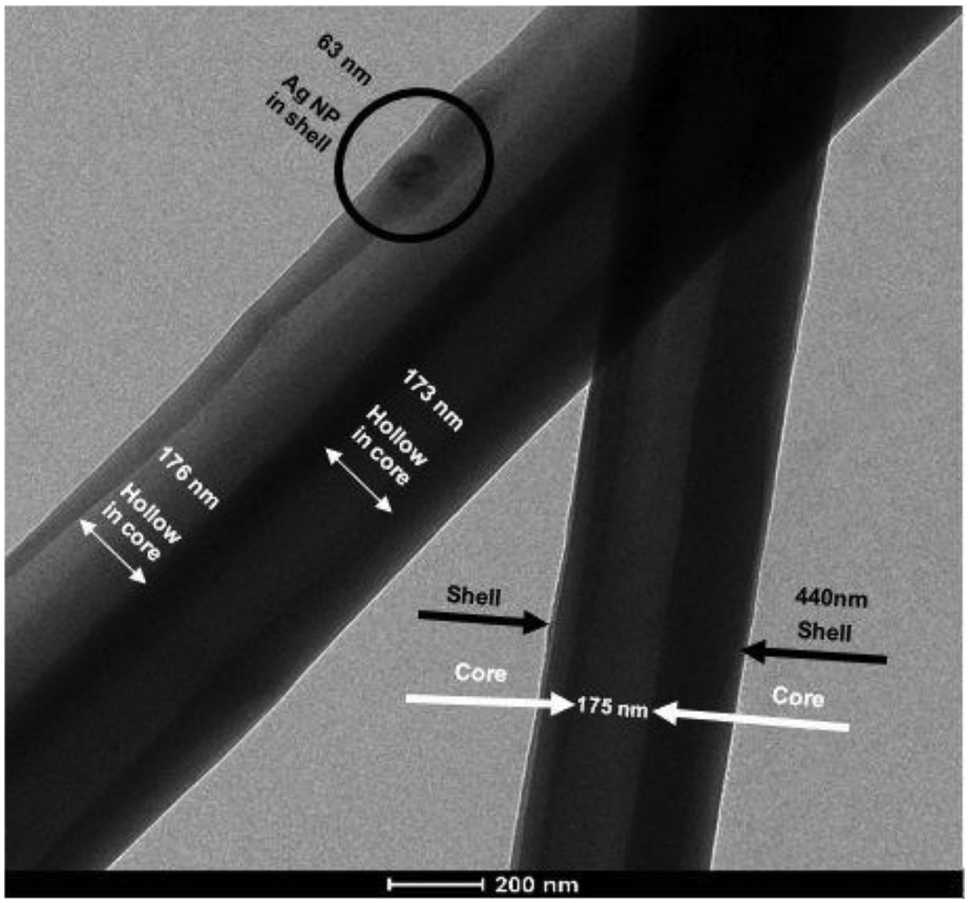

Fig. 4 TEM surface image of H5Ag5PLA5PU nanofiber (scale:200 nm)

the NH_2 group and the 2940 cm^{-1} peak denotes the CH_3 vibration. However, it is seen that the characteristic peaks of pure PVP nanofiber and Ag NP-doped hollow PLA/PU nanofibers do not overlap. FTIR graphic results both confirm the interaction and compatibility between PLA and PU and prove that the fibers are hollow and there is no other polymer in the structure.

DSC analysis of hollow PLA/PU/Ag NPs nanofibers

DSC curves that have shown thermal properties of Ag NP-doped hollow nanofibers are given in Fig. 6. Two different T_g values were observed for solid 5PLA5PU nanofibers. The T_g value for the PU nanofiber soft part is (-26 °C) and the T_g value for the PLA nanofiber is 61 °C [28]. The HPU showed a T_g value of around 75 °C for the hard part and a T_m value of around 268 °C for the hard part. A single T_g value around 61 °C was observed for the HPLA and H5PLA5PU nanofibers. Similarly, a single T_g value around 60 °C was observed in all Ag NP doped hollow nanofibers.

Table 3 EDX results of hollow PLA/PU/Ag NP nanofibers

Samples	H1Ag5PLA5PU	H3Ag5PLA5PU	H5Ag5PLA5PU
Ag NP amount (wt%)	1.12	3.49	5.63

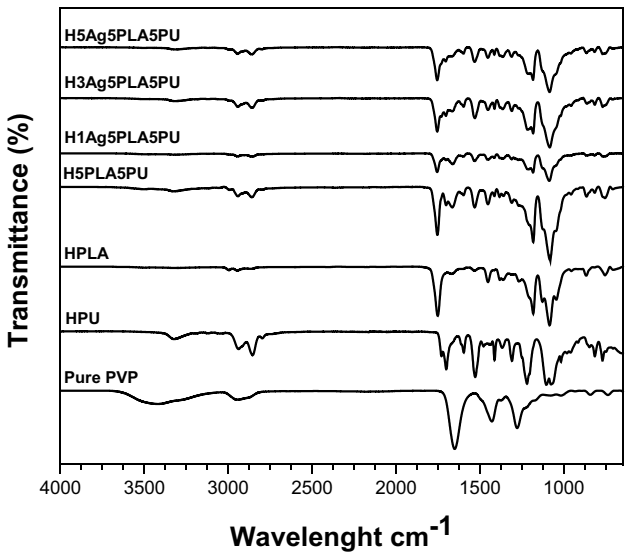

Fig. 5 FTIR spectra of hollow nanofibers

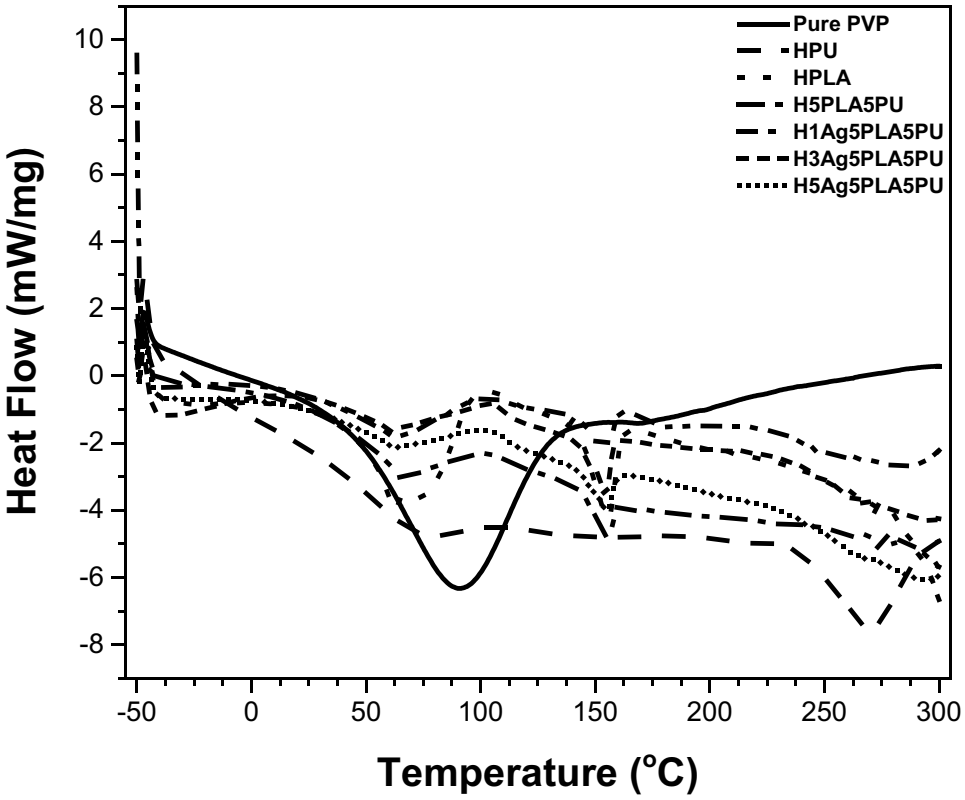

Fig. 6 DSC curves of hollow nanofibers

This is explained by the partial compatibility of the pure PLA polymer with the polyester or polyether group, which forms the soft part of the pure PU polymer [11]. Because the compatibility of polymer mixtures can be explained by the deviation of the T_g values of the components providing the mixture from the typical values of the components and shifting to each other.

The T_m value of the hard and loose segment was not observed in solid PLA/PU mixed nanofibers [28]. Likewise, a single T_m value around 150 °C was observed in HPLA and hollow PLA/PU nanofibers, as in solid PLA/PU blended nanofibers.

On the other hand, a wide T_m peak was observed at 92 °C due to the moisture on the pure PVP nanofiber and its characteristic structure [50, 51]. This value was not observed in any of the hollow nanofibers. Another point to be explained is that if distilled water remained in the hollow parts of the hollow PLA/PU nanofibers, a peak around 100 °C was observed due to the evaporation of the absorbed water. According to DSC results, there is no peak in hollow nanofibers at this temperature. In this case, it can be interpreted that there is no moisture in the structure of hollow nanofibers, and distilled water completely leaves the structure after drying. Because PLA/PU blended nanofibers do not hold water in their structures due to their hydrophobic structure [28]. In conclusion, the existence of hollow PLA/PU/Ag NP nanofibers has been proven by the findings of the characteristic thermal properties of polymers.

TGA analysis of hollow PLA/PU/Ag NPs nanofibers

TGA degradation temperature values of hollow Ag NP doped PLA/PU nanofibers are given in Table 4. It represents the decomposition temperature T_{d5} value corresponding to the 5% weight loss in TGA curves. In addition, T_{max} temperature values corresponding to the maximum degradation rate on the DTG derivative curves obtained from the TGA curves are also given. The amount of residue in the TGA analysis can be considered as another analysis that confirms both the amount of Ag NP in the structure and the emptying of the core of the produced nanofibers.

HPU nanofiber has shown a four-step thermal degradation curve. All Ag NP-doped hollow PLA/PU nanofibers also have exhibited a four-step degradation curve, just like the HPU nanofiber. This stepwise degradation has been associated with the degradation of soft and hard segments of polyurethane at different temperatures [28]. The first step is associated with the removal of moisture content from the structure. TGA values of all hollow PLA/PU nanofibers yielded results in the temperature range of HPLA and HPU nanofibers.

No sharp decrease in T_{deg5} temperatures has been observed. While a high decrease in thermal properties is expected due to the beaded structures, the thermal values due to the presence of Ag NP in the structures; showed similar thermal properties with smooth, and homogeneous (H5PLA5PU) hollow nanofiber. A significant increase in

Table 4 Thermal degradation values of hollow nanofibers

Samples	T_{max} (°C)				T_{d5} (°C)	Amount of Residue 600 °C (%wt)
	1st step	2nd step	3rd step	4th step		
PURE PVP	89.15	-	-	429.70	84.97	5.00
HPU	62.73	260.68	339.53	424.67	243.51	9.78
HPLA	52.91	305.83	-	-	249.57	4.61
H5PLA5PU	61.36	265.85	327.77	420.96	254.83	8.19
H1Ag5PLA5PU	66.10	293.84	341.65	422.59	237.22	9.33
H3Ag5PLA5PU	61.07	277.06	325.29	420.50	235.12	10.90
H5Ag5PLA5PU	58.13	272.87	321.10	420.08	241.83	13.72

T_{max1} and T_{max2} values in H1Ag5PLA5PU nanofiber was associated with an increase in resistance to temperature, and the late release time of homogeneously dispersed Ag NPs from fibers, due to less Ag agglomeration compared to other fibers.

It can be seen from the amount of residue that Ag NPs preserve their presence in the nanofiber structure at 600 °C. H5PLA5PU nanofiber left 8.19% residue between HPLA and HPU residual amounts. The amount of residue in the hollow PLA/PU/Ag NPs nanofiber also increased by the percentage (%) of Ag NPs in the nanofiber structure compared to the H5PLA5PU nanofiber.

No thermal properties of pure PVP were observed in the structure of Ag NP doped hollow PLA/PU nanofibers, and the amount of residue due to the presence of pure PVP nanofiber was not found.

Mechanical test results of hollow PLA/PU/Ag NPs nanofibers

The tensile strength [MPa] and elongation (%) graphs of hollow nanofibers are shown in Fig. 7. According to the information obtained from our previous study [28], all hollow blend nanofibers have a higher tensile strength and elongation at break value than the tensile strength (0.33 MPa) and elongation behavior (24.73%) of solid pure PLA nanofiber. This improved behavior is attributed to the fact that the use of PLA and PU polymers as a mixture improves the brittleness of PLA due to the superior elongation of PU [28]. While the tensile strength of the hollow H5PLA5PU nanofiber increased, its elongation of it displayed a slight increase [52–54]. The tensile strength of the H5PLA5PU nanofiber (7,20 MPa) was almost 2 times higher than the solid 5PLA5PU nanofiber (3,81 MPa) [28]. The tensile strength increases with the decrease in nanofiber diameter. While the diameter of the solid 5PLA5PU nanofiber was 1584 nm [28], the diameter of the H5PLA5PU nanofiber was 518 nm. In hollow nanofibers, the inner diameter can be obtained quite thin compared to the outer diameter. It has been reported that tensile strength values will increase with decreasing the diameter of the fiber, owing to the hollow channel volume fraction [52]. It was observed that converting to a hollow structure reduced the tension and friction between nanofibers [54]. This tendency resulted in increased elongation of the H5PLA5PU (41,65%) compared with 5PLA5PU (34,73%) nanofiber [28].

The mechanical properties of nanofibers are related to the distribution, regularity, and intensity of intramolecular and intermolecular interactions between polymer chains in the nanofiber matrix. Owing to the compatibility between PLA and PU polymer chains [28], intense hydrogen bonds formed between PLA/PU (blends) polymers were created high regularity. This contributed to the improvement of the mechanical properties of nanofibers. At the same time, the distribution of metal nanofillers in the polymer mixture directly affects the nanofiber mechanical properties [55–57]. It was observed that the tensile strength of hollow nanofibers decreased due to the hard structure of Ag NPs, but the elasticity values of nanofibers increased when the percentage of AgNPs was increased. Although 3% and 5% doped Ag NP nanofibers were lower than the elongation of 1% Ag NP doped nanofibers, they were higher than HPU, HPLA, and H5PLA5PU nanofibers. This result showed that the optimum value of the Ag NP additive amount affects the tensile strength and elongation properties of nanofibers. The excess AgNP loading (3% and 5%) (above the optimum value) reduced the molecular mobility, making the nanocomposite materials harder. In this case, hollow nanofibers with lower tensile strength than 1%Ag added nanofibers were formed. Exceeding the Ag NP optimum additive amount is considered a result of the uneven distribution and agglomeration of Ag NPs in the PLA/PU matrix. These results were supported by SEM images. Excess agglomeration formation and poor particle dispersion were associated with high AgNP content, which was caused between the polymers phase separation and weakened material bonding, resulting in poor mechanical properties. As a result, it can be attributed to positive interaction facilitating adequate interfacial adhesion for 1% AgNPs and PLA/PU (50/50, w/w) polymer blend.

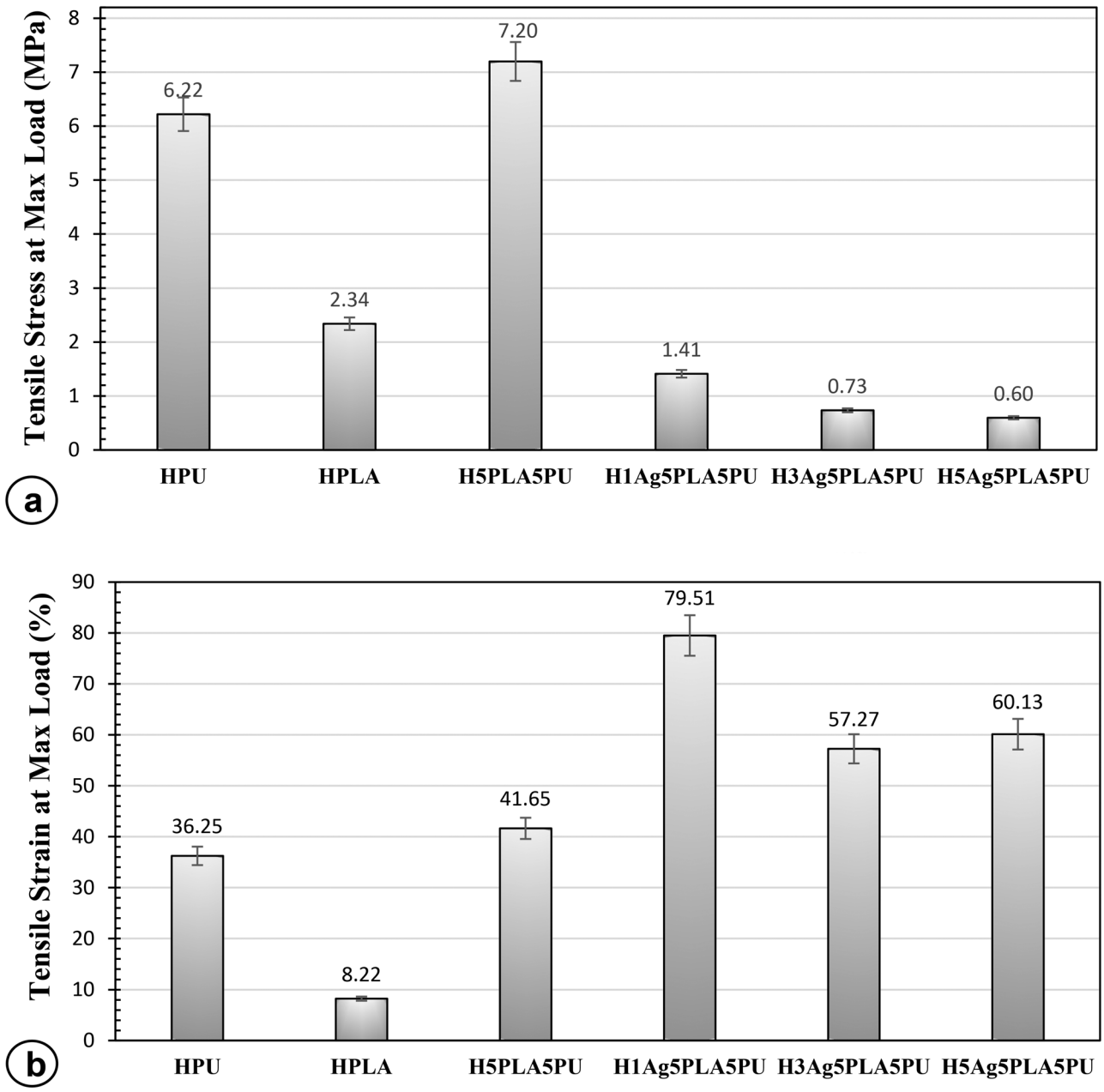

Fig. 7 **a** Graphs of tensile stress at max load (MPa) of hollow nanofibers **b** Graphs of tensile strain at max load (%) of hollow nanofibers

Additionally, the reduction in tensile strength was associated with also the presence of unwanted bead structures on the nanofibers seen in the SEM images. Due to the presence of knotted, lumpy, and polymer droplets (beads), these regions behaved like pure PLA [28] and exhibited poor tensile strength. On the contrary, elongation increases due to these regions and the hollow structure. Because in the presence of polyurethane, loose parts in the polymer bead structure can show elongation behavior. All Ag NP-doped nanofibers showed higher elongation values compared to H5PLA5PU nanofibers. H1Ag5PLA5PU nanofiber exhibited the highest elongation behavior [58]. At the same time, H1Ag5PLA5PU nanofiber has the highest tensile strength among Ag NP-doped hollow nanofibers. It has been attributed to the presence of smooth and bead-free H1Ag5PLA5PU nanofibers in SEM images. The elongation values of H3Ag5PLA5PU and H5Ag5PLA5PU nanofibers are very close to each other. The beaded structures observed in the surface images of these fibers in the SEM analysis are also quite similar to each other.

The strain–stress graphs in Fig. 8 show the plastic deformation of nanomaterials until fracture. At the same time,

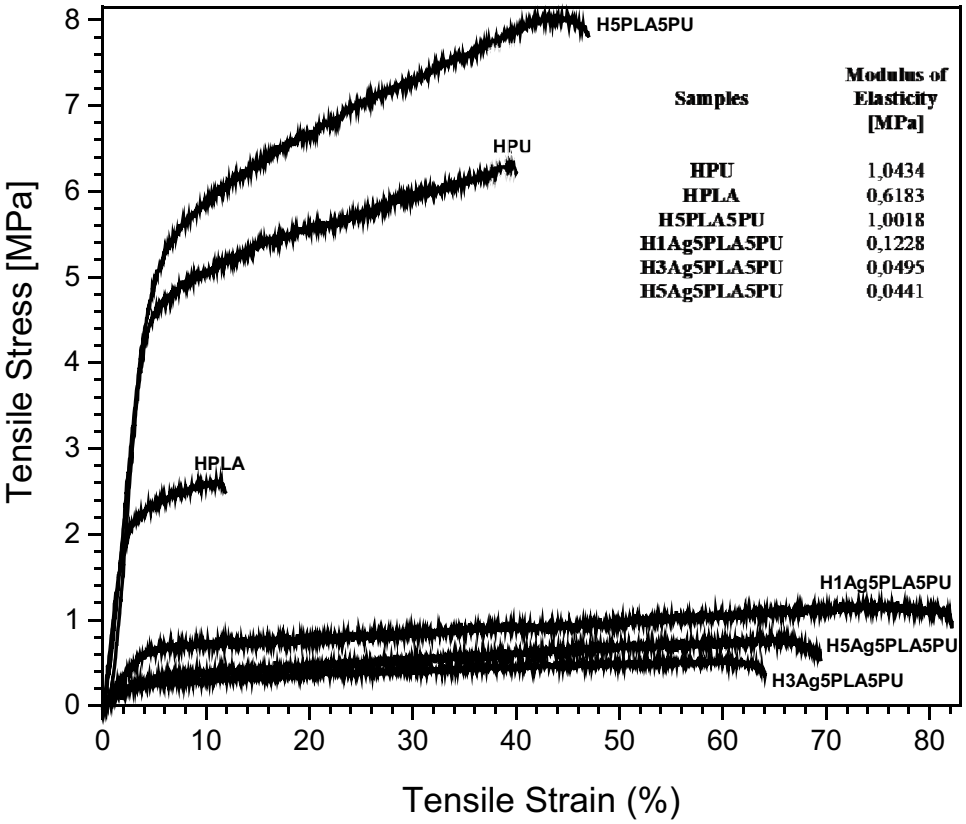

Fig. 8 Graphs of stress–strain of hollow nanofibers

the modulus of elasticity values also is given in Fig. 8. HPU, HPLA, and H5PLA5PU nanofibers exhibited linear proportionality with stress and strain, with a modulus of 1.0434, 0.6183, and 1.0018 MPa, respectively. It then increased parabolically with an increase in strain up to the peak stress point. After the strain exceeded this ultimate stress point, it displayed a brittle snap-break behavior. It was observed that the Ag NP-doped PLA/PU nanofibers (the lowest Ag NP contribution, respectively) had modulus values of 0.1228, 0.0495, and 0.0441 MPa. After reaching the highest stress point, they showed a constant elongation behavior by showing creep behavior without loss of strength.

Liquid absorption capacity and drying time of hollow PLA/PU/Ag NPs nanofibers

The values of the liquid absorbency capacity (%) and drying time (min) of the Ag NP doped hollow PLA/PU blend nanofibers are given in Table 5. The nanofibers produced from both polymer mixtures are hydrophobic nanomaterials with an angle of 120° [28]. While the liquid absorption capacity (LAC) is directly related to the interior space of the fibers, also it is related to the surface properties of the nanofibers and the presence of Ag NPs added to the structure. A sharp 2.75–3.25 (between) fold decrease was observed in nanofibers obtained by adding Ag NP into H5PLA5PU nanofiber, which has 756% absorbency capacity. This situation can be directly related to the fact that silver is a metal element. H3Ag5PLA5PU and H5Ag5PLA5PU nanofibers, which have finer fibrils than H1Ag5PLA5PU nanofibers, have low absorbency capacity due to the presence of polymeric beads in SEM images. The absorbency capacities of H3Ag5PLA5PU and H5Ag5PLA5PU nanofibers are 257% and 234%, respectively. As the amount of Ag NP in the structure and the bead structures increase, the absorbency capacity decreases. H1Ag5PLA5PU nanofiber, which has smooth, uniform nanofibers and the least amount of Ag NP, was produced as the nanomaterial with the highest absorbency with a value of 274%. Due to the presence of Ag NPs and the hydrophobic bead PLA/PU polymeric structures

Table 5 LAC (%) and drying time (min) of hollow PLA/PU/Ag NPs nanofibers

Samples	LAC (%)	Drying time (min)
H5PLA5PU	756	10
H1Ag5PLA5PU	274	8
H3Ag5PLA5PU	257	9
H5Ag5PLA5PU	234	9

on nanofibers, it becomes difficult for water molecules to reach the hollow structure. Ag NPs and beads repel water molecules. It is getting harder for water molecules to pass through the parts with Ag NP agglomeration and reach the hollow part.

According to the drying times, all Ag NP-doped hollow nanofibers dry at almost the same time and return to their original weight. Compared to the H5PLA5PU nanofiber, the nanofibers with a very low absorbency capacity, which can trap less liquid in their structure, providing drying in a shorter time.

When the water absorption capacity and drying times are evaluated in general, it is expected that if the hollow nanofibers are used in wound dressing applications, they will rapidly absorb the wound exudate with the capillary effect and absorb re-released exudate owing to dry quickly. With this circulation, it is predicted that while the PLA/PU/Ag nanofiber hydrophobic shell repels water molecules, the wound will heal quickly by keeping the environment moist, on the other hand, the PLA/PU/Ag nanofiber hollow core can absorbe the exudate.

Antibacterial test results of hollow PLA/PU/Ag NPs nanofibers

The antibacterial activity of Ag NP-doped hollow PLA/PU nanofibers against *E. coli, P. aeruginosa*, *and S. aureus* bacteria were investigated. According to the antibacterial activity (%) results, Ag NPs were highly effective against all bacterial species. Antibacterial activities of Ag NP-doped hollow PLA/PU nanofibers on *E. coli* are shown in Fig. 9. A numerical evaluation of *E. coli* colony counts of Ag NP-doped hollow PLA/PU nanofibers is given in Table 6.

During 0, 6, 12, and 24 h, many *E. coli* proliferation was observed in the H5PLA5PU nanofibers without Ag NPs, as expected. Therefore, these nanofibers were used as control samples. After adding Ag NPs, they showed 100% antimicrobial activity for *E. coli*. However, 1% Ag NP-doped PLA/

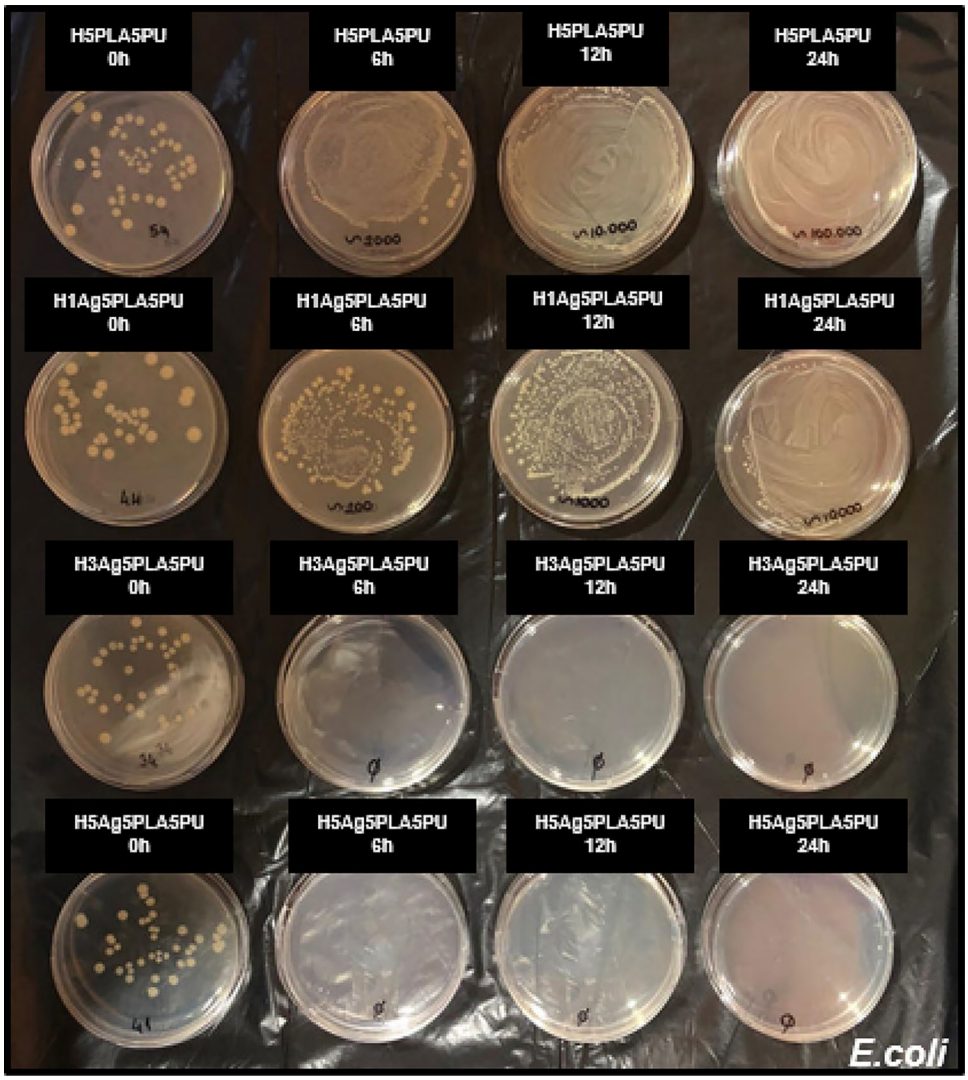

Fig. 9 Antibacterial effect of PLA/PU/Ag NP nanofibers on *E.coli* (from left to right: 0, 6, 12, 24 h, respectively) (from top to bottom, respectively: H5PLA5PU, H1Ag5PLA5PU, H3Ag5PLA5PU and H5Ag-5PLA5PU)

Table 6 *E.coli* count and antibacterial activity (%) in the presence of nanofibers

Samples	0 h	6 h	12 h	24 h	Antibacterial Activity (%)
H5PLA5PU	Average: 54 Std dev: 1.53	Average: ~ 2×10^3 (uncountable)	Average: ~ 10^4 (uncountable)	Average: ~ 10^5 (uncountable)	-
H1Ag5PLA5PU	Average: 44 Std dev: 1.53	Average: ~ 213 Std dev: 15.27	Average: ~ 10^3 (uncountable)	Average: ~ 10^4 (uncountable)	-
H3Ag5PLA5PU	Average: 34 Std dev: 2.00	Average: 0 Std dev: 0.00	Average: 0 Std dev: 0.00	Average: 0 Std dev: 0.00	100 for 6 h, 12 h and 24 h
H5Ag5PLA5PU	Average: 41 Std dev: 3.51	Average: 0 Std dev: 0.00	Average: 0 Std dev: 0.00	Average: 0 Std dev: 0.00	100 for 6 h, 12 h and 24 h

PU nanofiber was not effective on *E. coli* with time. As time progressed, the number of bacteria increased linearly.

When 3% Ag NP added PLA/PU nanofiber and 5% Ag NP added PLA/PU nanofiber were used, all *E.coli* were destroyed at the end of the 6th hour. The 100% antibacterial properties of these two hollow nanofibers continued until the end of the 24th hour. The H3Ag5PLA5PU and H5Ag5PLA5PU nanofibers can both be used as wound dressings for *E.coli*, provided that they are replaced at the end of 24 h. However, if a low Ag NP ratio is preferred, it is appropriate to use H3Ag5PLA5PU nanofibers as an antibacterial effective wound dressing for *E.coli*.

Antibacterial activities of Ag NP doped hollow PLA/PU nanofibers on *P.aeruginosa* are shown in Fig. 10. A numerical evaluation of *P.aeruginosa* colony counts of Ag NP doped hollow PLA/PU nanofibers is given in Table 7. For H5PLA5PU nanofiber without Ag NP, linear bacterial growth of *P.aeruginosa* was observed for 0, 6, 12, and 24 h by culturing on MHA agar. When 1% AgNP additive was added to the structure, antibacterial activity towards *P.aeruginosa* was observed at the end of the 6th hour. This activity continued until the end of the 12th hour. However, at the end of the 24th hour, an increase in bacteria was observed in the culture medium. The presence of Ag NPs has lost its effectiveness [20, 59].

When 3% and 5% Ag NP were added to the structure, 100% antibacterial activity, which started at the end of the 6th hour, continued until the end of the 24th hour. All Ag NP doped PLA/PU nanofibers can be used as an antibacterial effective wound dressing against *P.aeruginosa*. However, when H1Ag5PLA5PU nanofiber is used as an antibacterial effective wound dressing against *P.aeruginosa*, it should be changed at the end of the 12th hour; H3Ag5PLA5PU and H5Ag5PLA5PU nanofibers should be replaced after 24 h. In addition, when nanofibers with low Ag NP content in the structure are preferred to be used as an antibacterial effective wound dressing against *P.aeruginosa*; it is considered appropriate to use H3Ag5PLA5PU nanofibers, whose activity starts at the 6th hour and continues until the end of the 24th hour.

The antibacterial effects of Ag NP doped PLA/PU nanofibers on *S.aureus* are shown in Fig. 11. Bacteria counts were performed at 0, 6, 12, and 24 h intervals. A numerical comparison of *S. aureus* bacterial counts is given in Table 8. A significant time-dependent increase in the number of *S. aureus* was observed in the presence of H5PLA5PU nanofiber. This nanofiber was used as the control sample. H1Ag5PLA5PU and H3Ag5PLA5PU nanofibers did not show antibacterial activity against *S. aureus* at any of the 0, 6, 12, and 24 h intervals. Just like the control sample, a linear increase in the number of *S. aureus* was seen in the medium with time for these two hollow nanofibers. Since *S. aureus* is a Gram-positive bacteria species, it was thought that it is more difficult for Ag NPs to penetrate bacteria and prevent bacterial growth due to its thick cell wall [60].

Only H5Ag5PLA5PU nanofiber showed 100% antibacterial activity against *S.aureus*. This activity, which started at the 12th hour, lasted until the end of the 24th hour. Among Ag NP added PLA/PU nanofibers, it was deemed appropriate that the only nanofiber that can be used as an antibacterial effective wound dressing against *S.aureus* bacteria is H5Ag5PLA5PU nanofiber.

If the antibacterial analysis for Ag NP-doped hollow PLA/PU blended nanofibers is evaluated in general: for *E.coli* and *P.aeruginosa* bacterial species, it is predicted that H3Ag5PLA5PU nanofiber should be used and changed at the end of the 24th hour; also, H5Ag5PLA5PU nanofiber, which can be used simultaneously for 3 bacterial species, has been determined to can be used by changing it every 24 h.

Compared to other hollow nanofibers, H5Ag5PLA5PU seems to be a preferable electrospun mat as an antibacterial effective wound dressing since there is not a very high difference between its absorbency and drying time.

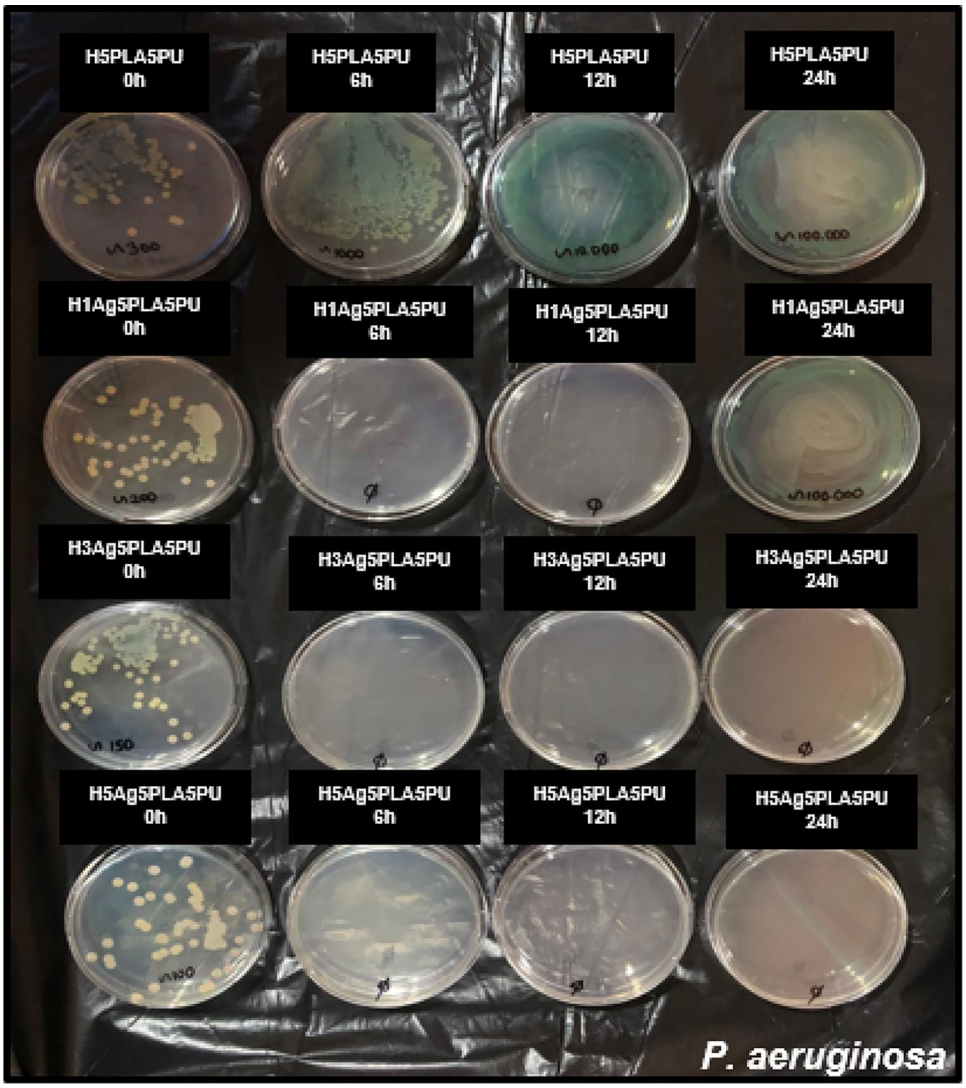

Fig. 10 Antibacterial effect of hollow PLA/PU/Ag NP nanofibers on *P. aeruginosa* (from left to right: 0, 6, 12, 24 h, respectively) (from top to bottom, respectively: H5PLA5PU, H1Ag5PLA5PU, H3Ag5PLA5PU and H5Ag-5PLA5PU)

Table 7 *P. aeruginosa* count and antibacterial activity (%) in the presence of nanofibers

Samples	0 h	6 h	12 h	24 h	Antibacterial Activity (%)
H5PLA5PU	Average: ~ 320 Std dev: 26.46	Average: ~ 10^3 (uncountable)	Average: ~ 10^4 (uncountable)	Average: ~ 10^5 (uncountable)	-
H1Ag5PLA5PU	Average: ~ 223 Std dev: 20.82	Average: 0 Std dev: 0.00	Average: 0 Std dev: 0.00	Average: ~ 10^5 (uncountable)	100 for 6 h and 12 h
H3Ag5PLA5PU	Average: ~ 155 Std dev: 13.23	Average: 0 Std dev: 0.00	Average: 0 Std dev: 0.00	Average: 0 Std dev: 0.00	100 for 6 h, 12 h and 24 h
H5Ag5PLA5PU	Average: ~ 103 Std dev: 15.28	Average: 0 Std dev: 0.00	Average: 0 Std dev: 0.00	Average: 0 Std dev: 0.00	100 for 6 h, 12 h and 24 h

Fig. 11 Antibacterial effect of hollow PLA/PU/Ag NP nanofibers on *S. aureus* (from left to right: 0, 6, 12, 24 h, respectively) (from top to bottom, respectively: H5PLA5PU, H1Ag5PLA5PU, H3Ag5PLA5PU and H5Ag-5PLA5PU)

Table 8 *S. aureus* count and antibacterial activity (%) in the presence of nanofibers

Samples	0 h	6 h	12 h	24 h	Antibacterial Activity (%)
H5PLA5PU	Average: 38 Std dev: 3.06	Average: ~ 10^4 (uncountable)	Average: ~ 10^5 (uncountable)	Average: ~ 10^6 (uncountable)	-
H1Ag5PLA5PU	Average: 36 Std dev: 1.53	Average: ~ 2×10^3 (uncountable)	Average: ~ 10^4 (uncountable)	Average: ~ 10^5 (uncountable)	-
H3Ag5PLA5PU	Average: 35 Std dev: 2.52	Average: 52 Std dev: 2.52	Average: 110 Std dev: 4.51	Average: ~ 10^5 (uncountable)	-
H5Ag5PLA5PU	Average: 32 Std dev: 2.52	Average: 19 Std dev: 1.53	Average: 0 Std dev: 0.00	Average: 0 Std dev: 0.00	100 for 12 h and 24 h

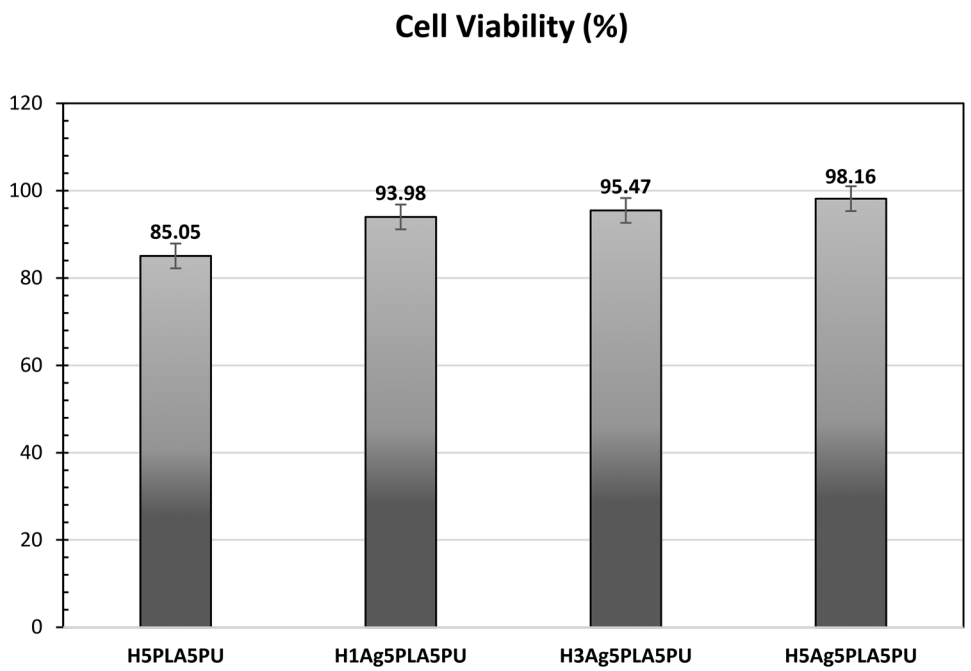

Fig. 12 Cell viability (%) of hollow PLA/PU/Ag NP nanofibers

Cytotoxicity (cell viability) test results of hollow PLA/PU/Ag NPs nanofibers

To examine the usability of all produced hollow nanofibers as an antibacterial effective wound dressing, the cytotoxicity test was performed using the direct contact test method cell viability (%) was calculated. The graphs showing the cell viability of the prepared Ag NP doped hollow nanofibers are given in Fig. 12.

Since the antibacterial test was performed for the 24th hour, the cytotoxicity test was also terminated at the end of the 24 h. The toxic effect of the positive control prepared in the test was recorded as 55.15% at the end of the 24th hour. It was deemed appropriate to evaluate PLA/PU/Ag NP nanofibers as non-toxic, provided that the cell viability (%) was at this value or higher. However, according to the information obtained from the literature; for the obtained Ag NP-doped PLA/PU nanofibers to be used as an antibacterial wound dressing, the cell viability should not be less than 70% [39].

H5PLA5PU nanofibers were evaluated as the negative control. Since PLA is a biocompatible polymer and PU is partially compatible with blood, high toxic effects are not anticipated. According to the results obtained, it was observed that all hollow PLA/PU/Ag NP nanofibers have an effect that supports cell growth. In addition, the decreased fiber diameter also supported the proliferation of cells [46]. H5Ag5PLA5PU nanofiber was found to be the highest cell growth support with a rate of 98.16%. According to the results obtained, all Ag NP-doped hollow nanofibers can be used as wound dressings since they are above 70% value.

According to the results of the cytotoxicity test and the antibacterial test results studied for three different bacterial species named *E. coli*, *P. aeruginosa*, and *S. aureus*; wound dressing, which is antibacterial for three bacterial species at the same time and contributes to fibroblast cell growth; It was reported to be H5Ag5PLA5PU nanofiber, provided it was replaced at the end of 24 h.

Conclusion

The antibacterial activity of these nanofibers against *E. coli, P. aeruginosa*, and *S. aureus* was investigated by the Agar plate colony counting method. H3Ag5PLA5PU nanofibers showed a100% antibacterial effect against gram-negative bacteria (*E. coli* and *P. aeruginosa*) until the end of the 24th hour. Against Gram-positive bacteria (*S.aureus*), only H5Ag5PLA5PU nanofibers showed 100% antibacterial effect. It has been reported that the most optimal nanomaterial to be used as a wound dressing with 100% antibacterial activity for up to 24 h against the 3 tested bacterial species is H5Ag5PLA5PU. In addition, this nanofiber exhibited the highest fibroblast cell viability with a value of 98.16%. This fiber was also observed to have the thinnest fiber diameters with a value of 484 nm. According to the SEM images, the surface structures of fibers are almost regular, but as the amount of Ag NP in the structure increased, the irregularities, the beaded structures, and the Ag agglomerations increased. The conductivity of the solutions increased with increasing Ag NP content; Due to the constant electrospinning conditions, a linear thinning of the diameters of the fibers was observed. According to the TEM image and

FTIR chemical analysis results, it has been proven that the fibers are hollow. It was observed that the H5Ag5PLA5PU nanofiber increased with an elongation value of 60.13% compared to that of the pure H5PLA5PU nanofiber. When used as a wound dressing, it is thought to can provide patient comfort with high elasticity. The presence of hollow structures, metallic nano additives, Ag NPs agglomeration, regularity of polymer chains, and polymeric bead structures on the nanofiber structure have affected the mechanical properties. The Ag NP-doped nanomaterials have exhibited a ductile behavior. In addition, the liquid absorption capacity of nanofibers decreased as the amount of Ag NP increased, mainly due to the agglomeration of Ag NPs and then the presence of beads. While agglomerated Ag metals repel water molecules, beaded PLA and PU structures with hydrophobic character also exhibit the repulsion behavior of water molecules. The LAC% decreased due to the water molecules that could not find a way to reach the hollow structure. However, there was no significant difference in drying times compared to pure H5PLA5PU nanofiber. Ag NP-doped nanofibers showed drying behavior in as little as 8–9 min. The residues in TGA proved the existence of Ag NPs in the structure, while also proving that the fibers were emptied. While DSC analysis gives information about the thermal properties of hollow nanofibers, it did not observe the thermal information of PVP on PLA/PU/Ag nanofibers. Thus, with this test also, the presence of hollow structures was proved. When all the results were evaluated, it was reported that wound dressing materials were developed with modern wound dressing properties and high antibacterial effects.

Acknowledgements We would like to thank Kocaeli University Scientific Research Project Unit (KOU BAP-Project Code FYL-2021-2425), which provided financial support for the necessary material supply and tests for this study.

Declarations

Conflicts of interest The authors declare no conflict of interest.

References

1. Değim Z (2008) Use of microparticulate systems to accelerate skin wound healing. J Drug Target 16:437–448
2. Ruszczak Z, Schwartz RA (2000) Modern aspects of wound healing: An update. Dermatol Surg 26:219–229
3. Hanna JR, Giacopelli JA (1997) A review of wound healing and wound dressing products. J Foot Ankle Surg 36:2–14
4. Mendez-Eastman S (2005) Wound dressing categories. Plastic Surg Nurs 25:95–99
5. Schultz GS, Sibbald RG, Falanga V, Ayello EA, Dowsett C, Harding K (2003) Wound bed preparation: A systematic approach to wound management. Wound Rep Reg 11:1–28
6. Costache MC, Qu H, Ducheyne P, Devore DI (2010) Polymer-xerogel composites for controlled release wound dressings. Biomaterials 31:6336–6343
7. Laurencin CT, Nair LS (2008) Nanotechnology and Tissue Engineering: The Scaffold, 1st edn. CRC, Boca Raton
8. Sacholos E, Czernuszka JT (2003) Making tissue engineering scaffold work. Review on the application of solid freeform fabrication technology to the production of tissue engineering scaffolds. Eur Cell Mater 5:29–40
9. Cai N, Dai Q, Wang Z, Luo X, Xue Y, Yu F (2014) Preparation and properties of nanodiamond/poly(lactic acid) composite nanofiber scaffolds. Fib Polym 15:2544–2552
10. Anderson KS, Lim SH, Hillmyer MA (2003) Toughening of polylactide by melt blending with linear low-density polyethylene. J Appl Polym Sci 89:1–12
11. Feng F, Ye L (2011) Morphologies and mechanical properties of polylactide/thermoplastic polyurethane elastomer blends. J Appl Polym Sci 119:2778–2783
12. Hong H, Wei J, Yuan Y, Chen FP, Wang J, Qu X, Liu CS (2011) A novel composite coupled hardness with flexibleness polylactic acid toughen with thermoplastic polyurethane. J Appl Polym Sci 121:855–861
13. Lee K, Lee B, Kim C, Kim H, Kim K, Nah C (2005) Stress-strain behavior of the electrospun thermoplastic polyurethane elastomer fiber mats. Macromol Res 13:441–445
14. Janik H, Marzec M (2015) A review: fabrication of porous polyurethane scaffolds. Mater Sci Eng C 48:586–591
15. Tatai L, Moore TG, Adhikari R, Malherbe F, Jayasekara R, Griffiths L, Gunatillake PA (2008) Thermoplastic biodegradable polyurethanes: The effect of chain extender structure on properties and in-vitro degradation. Biomaterials 28:5407–5417
16. Kim SE, Heo DN, Lee JB, Kim JR, Park SH, Jeon SH, Kwon K-II (2009) Electrospun gelatin/polyurethane blended nanofibers for wound healing. Biomed Mater 4:044106–044117
17. Jatoi AW, Kim IS, Ni QQ (2018) Ultrasonic energy-assisted coloration of polyurethane nanofibers. Appl Nanosci 8:1505–1514
18. Lamba NMK, Woodhouse KA, Cooper SL (1998) Polyurethanes in biomedical applications, 1st edn. Routledge, Roca Boston
19. Khoza PB, Moloto MJ, Sikhwivhilu LM (2012) The effect of solvents, acetone, water, and ethanol, on the morphological and optical properties of ZnO nanoparticles prepared by microwave. J Nanotechnol 195106:1–6
20. Nguyen TTT, Chung OH, Park JS (2011) Coaxial electrospun poly(lactic acid)/chitosan (core/shell) composite nanofibers and their antibacterial activity. Carbohyd Polym 86:1799–1806
21. Sun B, Duan B, Yuan X (2006) Preparation of core/shell PVP/PLA ultrafine fibers by coaxial electrospinning. J Appl Polym Sci 102:1–7
22. Jannesari M, Varshosaz J, Morshed M, Zamani M (2011) Composite poly(vinyl alcohol)/poly(vinyl acetate) electrospun nanofibrous mats as a novel wound dressing matrix for controlled release of drugs. Int J Nanomed 6:993–1003
23. Merrell JG, McLaughlin SW, Tie L, Laurencin CT, Chen AF, Nair LS (2009) Curcumin loaded Poly(ε-Caprolactone) nanofibers: diabetic wound dressing with antioxidant and anti-inflammatory properties. Clin Exp Pharmacol Physiol 36:1149–1156
24. Kim G, Park J, Park S (2007) Surface-treated and multilayered poly(ε-caprolactone) nanofiber webs exhibiting enhanced hydrophilicity. J Polym Sci Part B Polym Phys 45:2038–2046
25. Li L, Peng S, Lee JKY, Ji D, Srinivasan M, Ramakrishna S (2017) Electrospun hollow nanofibers for advanced secondary batteries. Nano Energy 39:111–139
26. Fong J, Wood F (2007) Nanocrystalline silver dressings in wound management: A review. Int J Nanomed 1:441–449
27. Rai M, Yadav A, Gade A (2009) Silver nanoparticles as a new generation of antimicrobials. Biotechn Adv 27:76–83
28. Samatya Yilmaz S, Aytac A (2021) Poly(lactic acid)/polyurethane blend electrospun fibers: structural, thermal, mechanical, and surface properties. Iran Polym J 30:873–883

29. Samatya Yilmaz S, Aytac A (2021) The effect of different compatibilizers on the properties of prepared poly(lactic acid)/polyurethane nanofibers by electrospinning. J Indust Text 51:8428S-8451S
30. Lee GH, Song JC, Yoon KB (2010) Controlled wall thickness and porosity of polymeric hollow nanofibers by coaxial electrospinning. Macromol Res 18:571–576
31. Zhang X, Wang Y, Guo D, Wang Y (2012) The Morphology of The Hollow PAN Fibers through Electrospinning. ASRI Proced 3:236–241
32. Li D, Xia Y (2004) Direct fabrication of composite and ceramic hollow nanofibers by electrospinning. Nano Lett 4:933–938
33. Khil MS, Cha D-II, Kim HY, Kim IS, Bhattarai N (2003) Electrospun nanofibrous polyurethane membrane as wound dressing. J Biomed Mater Res B Appl Biomater 67:675–679
34. Hajikhani M, Emam-Djomeh Z, Askari G (2021) Fabrication and characterization of mucoadhesive bioplastic patch via coaxial polylactic acid (PLA) based electrospun nanofibers with antimicrobial and wound healing application. Int J Bio Macromol 172:143–153
35. Ge L, Li Q, Wang M, Ouyang J, Li X, Xing MMQ (2014) Nanosilver particles in medical applications: synthesis, performance, and toxicity. Inter J Nanomed 9:2399–2407
36. Wong KKY, Liu X (2010) Silver nanoparticles - The Real "Silver Bullet" in Clinical Medicine? Med Chem Comm 1:125–131
37. Gibbard J (1937) Public health aspects of the treatment of water and beverages with silver. Am J Publ Health Nat Health 27:112–119
38. Tian J, Wong KKY, Ho CM, Lok CN, Yu WY, Che CM, Chiu JF, Tam PKH (2007) Topical delivery of silver nanoparticles promotes wound healing. Chem Med Chem 2:129–136
39. Alippilakkotte S, Kumar S, Sreejith L (2017) Fabrication of PLA/Ag nanofibers by green synthesis method using momordica charantia fruit extract for wound dressing. Appl Coll Surf A Physicochem Eng Aspects 529:771–782
40. Tijing LD, Ruelo MTG, Amarjargal A, Pant HR, Park CH, Kim CS (2012) One-step fabrication of antibacterial (silver nanoparticles/poly(ethylene oxide))– polyurethane bicomponent hybrid nanofibrous mat by dual-spinneret electrospinning. Mater Chem Phys 134:557–561
41. Ng IS, Ooi CW, Liuc BL, Peng CT, Chiu CY, Chang YK (2020) Antibacterial efficacy of chitosan- and poly(hexamethylene biguanide)- immobilized nanofiber membrane. Inter J Biol Macromol 154:844–854
42. Lan X, Liu Y, Wang Y, Tian F, Miao X, Wang H, Tang Y (2021) Coaxial electrospun PVA/PCL nanofibers with dual release of tea polyphenols and ε-poly (L-lysine) as antioxidant and antibacterial wound dressing materials. Inter J Pharm 601:120525–120535
43. Guo Y, An X, Fan Z (2021) Aramid nanofibers reinforced polyvinyl alcohol/tannic acid hydrogel with improved mechanical and antibacterial properties for potential application as wound dressing. J Mechan Behav Biomed Mater 118:104452–104466
44. Ali SW, Rajendran S, Joshi M (2011) Synthesis and characterization of chitosan and silver loaded chitosan nanoparticles for bioactive polyester. Carbohydr Polym 83:438–446
45. Wu JY, Ooi CW, Song CP, Wang CY, Liu BL, Lin GY, Chiu CY, Chang YK (2021) Antibacterial efficacy of quaternized chitosan/poly (vinyl alcohol) nanofiber membrane crosslinked with blocked diisocyanate. Carbohydr Polym 262:117910–117921
46. Movahedi M, Asefnejad A, Rafienia M, Khorasani MT (2020) Potential of novel electrospun core-shell structured polyurethane/starch (hyaluronic acid) nanofibers for skin tissue engineering: in vitro and in vivo evaluation. Inter J Biol Macromol 146:627–637
47. Zekry SSA, Abdellatif A, Azzazy MHE (2020) Fabrication of pomegranate/honey nanofibers for use as antibacterial wound dressings. Wound Med 28:100181–100189
48. Deniz AE, Vural HA, Ortaç B, Uyar T (2011) Gold nanoparticle/polymer nanofibrous composites by laser ablation and electrospinning. Mater Lett 65:2941–2943
49. Dhumale VA, Gangwar RK, Datar SS, Sharma RB (2012) Reversible aggregation control of polyvinylpyrrolidone capped gold nanoparticles as a function of pH. Mater Express 2:311–318
50. Akhgari A, Ghalambor Dezfuli A, Rezaei M, Kiarsi M, Abbaspour M (2016) The design and evaluation of a fast-dissolving drug delivery system for loratadine using the electrospinning method. Jundishapur J Nat Pharm Products 11:33613–33623
51. Sethia S, Squillante E (2004) Solid dispersion of carbamazepine in PVP K30 by conventional solvent evaporation and supercritical methods. Inter J Pharm 272:1–10
52. Moattari RM, Mohammadi T, Rajabzadeh S, Dabiryan H, Matsuyama H (2021) Reinforced Hollow Fiber Membranes: A Comprehensive Review. J Taiwan Inst Chem Eng 122:284–310
53. Najafi SJ, Gharehaghaji AA, Etrati SM (2016) Fabrication and characterization of elastic hollow nanofibrous PU yarn. Mater Design 99:328–334
54. Shirolkar N, Maffe A, DiLoreto E, Arias-Monje PJ, Lu M, Ramachandran J, Gulgunje P, Gupta K, Park JG, Shih KC, Kirmani MH, Sharits A, Nepal D, Nieh MP, Liang R, Tsotsis T, Kumar S (2021) Multichannel hollow carbon fibers: processing, structure, and properties. Carbon 174:730–740
55. Rozilah A, Jaafar CNA, Sapuan SM, Zainol I, Ilyas RA (2020) The effects of silver nanoparticles compositions on the mechanical, physiochemical, antibacterial, and morphology properties of sugar palm starch biocomposites for antibacterial coating. Polymers 12:2605–2621
56. Abutaliba MM, Rajeh A (2021) Enhanced structural, electrical, mechanical properties and antibacterial activity of Cs/PEO doped mixed nanoparticles (Ag/TiO_2) for food packaging applications. Polym Testing 93:107013–107025
57. Su CH, Chen HL, Ju SP, Chen HY, Shih CW, Pan CT, You TD (2020) The mechanical behaviors of polyethylene/silver nanoparticle composites: an ınsight from molecular dynamics study. Sci Rep 10:7600–7613
58. Yadav K, Jha S, Jassal M, Agrawal AK (2019) Internally coated highly conductive and stretchable AgNW-PU hollow fibers. Polymer 169:46–51
59. Lv H, Cui S, Yang Q, Song X, Wang D, Hu J, Zhou Y, Liu Y (2021) AgNPs-ıncorporated nanofiber mats: relationship between AgNPs Size/content, silver release, cytotoxicity, and antibacterial activity. Mater Sci Eng C 118:111331–111340
60. Feng QL, Wu J, Chen GQ, Cui FZ, Kim TN, Kim JO (2000) A mechanistic study of the antibacterial effect of silver ıons on escherichia coli and staphylococcus aureus. J Biomed Mater Res 52:662–668